MUC3A Promotes Non-Small Cell Lung Cancer Progress via Activating NFκB Pathway and Attenuates Radiosensitivity

Yingming Sun
Wuhan University Zhongnan Hospital
Xiaoge Sun
Wuhan University Zhongnan Hospital
Chengcheng You
Wuhan University Zhongnan Hospital
Shijing Ma
Wuhan University Zhongnan Hospital
Yuan Luo
Wuhan University Zhongnan Hospital
Shan Peng
Wuhan University Zhongnan Hospital
Fang Tang
Wuhan University Zhongnan Hospital
Xiaoli Tian
Wuhan University Zhongnan Hospital
Feng Wang
Wuhan University Zhongnan Hospital
Zhengrong Huang
Wuhan University Zhongnan Hospital
Hongnv Yu
Dalian University Affiliated Xinhua Hospital
Yu Xiao
Wuhan University Zhongnan Hospital
Xiaoyong Wang
Wuhan University Zhongnan Hospital
Junhong Zhang
Wuhan University Zhongnan Hospital
Yan Gong
Wuhan University Zhongnan Hospital
Conghua Xie (chxie_65@whu.edu.cn)

Wuhan University Zhongnan Hospital https://orcid.org/0000-0001-6623-9864

Research

Keywords: NSCLC, radiosensitivity, MUC3A, NFκB

Posted Date: August 14th, 2020

DOI: https://doi.org/10.21203/rs.3.rs-57292/v1

Abstract

Background: MUC3A is highly expressed in lung adenocarcinoma, but its functions and effects on clinical outcomes are not well understood.

Methods: Tissue microarray was used to analysis the relathionship between MUC3A and clinicalpathological charcristics of lung adenocarcinoma; Colony formation and MTT array ware used to detect cell proliferation; WB applied to investigate the protein amount; Transwell was applied to evaluate cell invasion; IF was used to observe the location and expression of targeted proteins; IP was use to prove the binding of proteins. Mcherry-GFP-LC3 II adenovirus and TEM were performed to observe cell autophagy. Xnograft mouse model were used to investigate the effect of MUC3A in vivo.

Result: 92 patients' tumor samples indicated that high expression of MUC3A was associated with poor prognosis, advanced staging, and low differentiation. Co-immunoprecipitation results revealed that MUC3A interacted with RELA. MUC3A activated the NFκB pathway via promoting RELA phosphorylation and interfering the binding of RELA to IκB. MUC3A knockdown significantly suppressed cell proliferation and induced G1 arrest. MUC3A deficiency increased radiation-induced DNA double strain breaks via impairing the BRCA-1/RAD51 pathway and nuclear translocation of P53 and XCRR6. Moreover, MUC3A deficiency induced autophagy in lung cancer cells. MUC3A knockdown significantly suppressed tumor growth in xenograft model and had a synergistic effect with radiation. Less nuclear translocation of RELA and P53 was also observed in tumor tissue in vivo.

Conclusion: MUC3A was a potential oncogene, and its high expression was associated with unfavorable clinical outcomes. Patient with high expression of MUC3A should be more frequent follow-up and might benefit less from radiotherapy.

Background

Non-small cell lung cancer (NSCLC) is one of the most common human malignancies with the highest mortality rate over the past 30 years [1]. Sixty percent of NSCLC patients are diagnosed at advanced stages, and more than 50% of NSCLC patients need radiotherapy during their disease course. Previous studies showed that local control was associated with survival benefits [2–5]. The ultimate goal of radiotherapy is to achieve local tumor control while reducing damage to surrounding normal tissues [6]. Previous studies suggested that a radiation dose of more than 84 Gray (Gy) was required for 50% tumor control within three years and that a biological effect dosage (BED) more than 100 Gy for stereotactic ablation radiotherapy was necessary to achieve more than 90% local control [7]. These data indicated that higher BED resulted in better local control. Although the continuous improvement of techniques [8], the therapeutic effects of radiotherapy on NSCLC is still unsatisfactory, with the 5-years survival rate only 16.1%. Therefore, it is urgent to improve BED and predict radiotherapy prognosis [9, 10].

Many mucins (MUCs) were reported as biomarkers to identify and monitor the progression of lung cancer, and their abnormal expression was involved in tumor progression and metastasis by altering various

signaling pathways [11–13]. MUC1 was overexpressed in 86.3% adenocarcinomas, 39.1% squamous cell carcinomas, and 74.1% other NSCLC subtypes, and an independent prognostic factor for overall survival (OS) and disease-free survival (DFS) in patients with stage IB NSCLC [14, 15]. MUC4 was significantly up-regulated in patients with stage I (138 cases) and II (17 cases) lung adenocarcinoma (LUAD), and its high levels in early-stage patients correlated with shorter DFS and OS [16]. MUC5AC was reported to be highly expressed in 26.2% (16/61) of patients with stage I/II NSCLC and showed a relationship to clinicopathological profiles and prognosis [17]. These studies suggested a close correlation between MUCs and lung cancer pathogenesis, development, and prognosis.

MUC3A is a membrane-associated MUC with glycosylation and expressed in various epithelial cells. Previous researches indicated that MUC3A contained a sperm protein, enterokinase, and agrin (SEA) and epithelial growth factor (EGF) domain and functioned via ligand binding and intracellular signaling pathways [18]. MUC3A is rarely expressed in normal pulmonary epithelial cells, making it a promising tumor biomarker for lung cancer [19]. In breast, pancreatic, gastric, colorectal, prostate, and renal cancers, abnormally high MUC3A levels were correlated with poor clinical outcomes [20–25]. Based on the Oncomine database, we found that MUC3A was overexpressed in NSCLC. However, the relationship between MUC3A and the clinical prognosis is still to be explored.

Currently, the mechanism of MUC effects on the occurrence and development of NSCLC was still unclear. This may result from the complex biological properties of MUCs and their complex and even opposite functions in different cell types [25]. Our results revealed that MUC3A was a potential oncogene and that its high expression was associated with unfavorable clinical outcomes in NSCLC patients. MUC3A deficiency inhibited NSCLC cell proliferation, migration, and invasion via downregulating the NFκB pathway. MUC3A deficiency also increased the radiosensitivity of NSCLC cells both *in vivo* and *in vitro*. Our studies suggested MUC3A as a prognostic marker and therapeutic target.

Methods

Tissue microarray and bioinformatics analysis

The lung cancer tissue microarray was purchased from Outdo (Shanghai, China), containing 92 LUAD tissues and paired para-carcinoma tissues. Both intensity and positive percentage of immunohistochemistry (IHC) were used to examine MUC3A expression: the IHC H-score (values 0-400) = the scores for intensity of positive staining (negative = 0, weak = 1, moderate =2, or strong = 3) × the percentage of positive-stained cells × 100. A total of 156 cases of Hou Lung lung cancer data from Oncomine was used to analyze the expression of MUC3A in various lung cancer histological types and normal tissue. A TCGA based database *http://gepia.cancer-pku.cn.* To analysis, the Pearson correlation of two genes. A total of 156 cases of MUC3A expression in the normal and various lung cancer tissues was analyzed in the online database Oncomine. R language package to analyze the Pearson correlation of MUC3A and RELA log2 expression.

Cells

The NCI-H1975 and NCI-H1299 cell lines were purchased from the Type Culture Collection (Chinese Academy of Sciences, Shanghai, China) with the short tandem repeat sequencing authentication (Cellcook Biotech, Guangzhou, China, Figure S1-2). Both cell lines were cultured in RPMI-1640 medium (HyClone, USA) with 10% fetal bovine serum (HyClone), 100 units/ml penicillin and 100 μg/ml streptomycin (HyClone) at 37 °C with 5% CO_2.

Cell viability assay

The cells were seeded in 96-well plates (7,000 cells/well) and cultured for 5 days. After adding 10 μl CCK8 (Dojindo, Japan) to each well and incubating at 37 °C for 2 h, the absorbance at 450 nm was measured by the Rayto-6000 system (Rayto, China), and normalized to that of RPMI-1640 medium as control.

Colony formation assay

For cell proliferation, we seeded 50 cells to each well of 12-well plates for 7 days, then fixed with 4% paraformaldehyde (PFA) and stained with crystal violet. For radiation sensitivity, 100, 200, 400, 1,000, 2,000 and 10,000 cells were seeded in 6-well plates. The cells were then irradiated at 0, 1, 2, 4, 6, 8, and 10 Gray (Gy) with the Small Animal Radiation Research Platform (SARRP, 204 kV, PXI X-RAD 225Cx, CT, USA) from a photon beam. After 15 days, the colonies were fixed with 4% PFA for 15 min and stained with crystal violet. The cells were photographed, and the numbers of colonies were counted. A “multitarget-single hitting” model was applied to fit the survival curve.

Cell cycle assay

After starving for six h, the cells were harvested, fixed with cold ethanol overnight, and then incubated with propidium iodide and RNAse (BD, USA) in the dark for 15 min. The stained cells were assessed by flow cytometry (FACS AriaIII, BD, USA) and analyzed by FlowJo vX.0.7 software.

Cell apoptosis assay

The cells cultured on 24-mm coverslips were fixed by 4% PFA at room temperature for 30 min. After incubating with 0.1% Triton X-100 for 2 min, the TUNEL assay was performed according to the manufacturer’s instruction (Roche, Germany). The nuclei were labeled with DAPI at 2 μg/ml, and the immunofluorescence staining was analyzed by a fluorescence microscope (Olympus IX 73 DP80, Japan).

Modified Boyden chamber migration and invasion assay

The cells were seeded into the upper chambers of 12-well plates (1.5×10^5 cells/well) and cultured for 24 h. For invasion assay, the transwell membranes were precoated with Matrigel (1:40 dilution, Corning, USA) at 37 °C. After 24h, the cells were fixed with 4% PFA and stained with 0.1% crystal violet. The invaded and migrated cells were counted at five random fields per chamber under a phase-contrast microscope (DC 300F, Leica, Germany).

Immunoblotting analysis

The cells were lysed in RIPA buffer containing protease inhibitor and phosphatase inhibitor (Sigma-Aldrich, USA) on ice for 30 min. The cell lysates were centrifuged at 12,000 g for 15 min, and the supernatants were collected. The protein concentration was determined by Bradford protein assay (Bio-Rad, USA). The total proteins were separated using 7.5-12.5% SDS-PAGE (Bio-Rad) and transferred to a PVDF membrane (Millipore, USA). TBST with 5% milk was used to block non-specific binding sites. The dilution of antibodies for WB has been list in Table S1-2. The immunoreactive proteins were detected by enhanced chemiluminescence.

Immunofluorescence staining

The NSCLC cells were seeded on 24-mm coverslips, fixed with 4% PFA for 30 min, penetrated with 0.1% Triton X-100 and blocked with 5% BSA at room temperature for 1 h. After incubated with primary antibody at 4 °C overnight, the cells were incubated with Cy3-labelled or FITC-labelled secondary antibodies at room temperature for 1 h. The nuclei were labeled with DAPI (2 μg/ml). The immunofluorescence staining was examined using a fluorescence microscope (IX 73 DP80, Olympus, Japan) or a laser confocal microscope (C2, Nikon, Japan). The mean density was applied to semi-qualified by Image-Pro Plus 6.0.

Co-immunoprecipitation

The NSCLC cells were lysed in RIPA buffer containing protease inhibitor and phosphatase inhibitor (Sigma-Aldrich, USA) on ice for 30 min. The cell lysates were centrifuged at 12,000 g for 15 min to collect the supernatant. Co-immunoprecipitation was performed as the protocol of BeaverBeads™ Protein A/G Immunoprecipitation Kit (Beaverbio, Suzhou, China).

Autophagy investigation

Mcherry-GFP-LC3 II adenovirus infection

3×10^5 cells were seeded in 6-well plate; once the cells stuck to the wells, Mcherry-GFP-LC3 II (Beyotime Ltd, Beijing, China) adenovirus was infected into cells. The cells were treated with 4 Gy X-ray 24 h after infection. Fluorescence microscope (Olympus IX 73 DP80, Japan) was used to observe the fluorescence 12 h after irradiation. After infection of cells with Ad-mCherry-GFP-LC3B adenovirus, mCherry-GFP-LC3B was presented in the cytoplasm with diffuse yellow fluorescence (a combination of mCherry and GFP) in the absence of autophagy. In the case of autophagy, mCherry-GFP-LC3B accumulated on the autophagic membrane in the form of yellow spots (LC3B dot or punctae) under fluorescence microscopy; when the autophagosome was fused to lysosomes, as a consequence of GFP fluorescence quenching under acidic environment, it appeared as red spots.

Transmission electron microscopy (TEM)

Four hours after irradiation, the cells were washed three times with PBS and then collected by cell scraper, centrifuged at 2000 r/min for 5 min, discarded the supernatants. The cell pellets were fixed with 2.5% glutaraldehyde for 1h, then post-fixed with 1% osmium tetroxide buffer for 1 h. Subsequently, an ascending series of alcohol were performed for dehydration before embedding samples in Araldite. Ultrathin sections were observed by TEM (HT7700, Hitachi, Japan, 100kV).

Tissue assay

The microarrays including 92 pairs of lung adenocarcinoma and corresponding non-tumor tissues are purchased from BioChip (Shanghai, China), the samples come from National Human Genetic Resources Sharing Service Platform (2005DKA21300), all the dots on the chip were detected by IHC with survival information and included in univariate and multivariate survival analyses (Table S3). H-score applied to semi-qualify the IHC results; the representative images of 4 different staining intensities were shown in Figure 1A.

Animals

Six-week-old female *BALB-C/NULL* mice (Vital River Laboratory Animal Technology Co., Ltd, Beijing, China) were housed in a specific pathogen-free, temperature, and humidity-controlled environment with food and water in their cages. All animal experiments were performed according to the Wuhan University Animal Care Facility and the National Institutes of Health Guidelines.

In vivo assay

Approximately 5×10^6 H1975-GFP cells were harvested, resuspended in 100 μl PBS, and injected subcutaneously into the right flank of each mouse. Treatment was commenced when the tumor size reached approximately 100 mm^3. The mice were randomized into four groups and treated as follows: control, MUC3A KD group, control with radiation group (20 Gy/2 f, Small Animal Irradiation Research Platform SARRP, PXI X-RAD 225Cx, CT, USA), and MUC3A KD with radiation group. The size of the subcutaneous tumors and weight of the mice were recorded every day. Before the mice were radiated, we applied X-ray fluoroscopy to confirm the completed loci in the irradiated field. An animal *in vivo* imaging system was used to evaluate the size of the tumor at Day 7 and 14 after radiotherapy. Tumor volume (V) was calculated according to the formula: $\pi/6 \times \text{length} \times \text{width}^2$. The mice were sacrificed when the following points were reached: 1, tumor size reached 1,500 mm^3; 2, the tumor influenced breathing, eating, walking, and any other physiologic functions; 3, the tumor surface appeared to have anabiosis.

The tissues from the tumor-bearing mice were fixed in 4% PFA at four ℃ overnight and embedded into paraffin (Paraplast, Sigma-Aldrich) using tissue processor (Thermo Fisher Scientific, Loughborough, UK). Paraffin sections (5 μm) were cut with a rotation microtome (Thermo Fisher Scientific, Bremen, Germany). The images were collected by Versa 8 (Leica, Germany). IHC was followed by the protocol described. The integrated optical density (IOD) of the immunohistochemistry (IHC) section was calculated by Image-Pro Plus 6.0.

Statistical analyses

Each experiment was performed in triplicates and data presented in the representation of 3 individual experiments. A two-tailed Student's t-test and one-way analysis of variance (ANOVA) were used to evaluate the statistical significance of different groups. Statistical analyses were performed with SPSS 16.0. $P < 0.05$ were considered as statistical significance.

Results

MUC3A was highly expressed in lung cancer and relevant to poor OS

MUC3A expression in the normal and various lung cancer tissues was analyzed in the online database Oncomine. We found that MUC3A levels in LUAD and squamous cell carcinoma were significantly higher than those in normal lung tissues ($p < 0.01$, Figure S3A). The abnormal expression of MUC3A in cancer tissues suggested that MUC3A might involve in tumorigenesis and be associated with poor prognosis in lung cancer patients. Owing to mucin usually elevated expresses in adenocarcinoma, we used LUAD tissue microarray (Figure S3B) and particular scoring system (Figure 1A) to further experimentally confirmed that MUC3A protein levels are significantly up-regulated in LUAD tissues than in normal lung tissues ($P < 0.001$, Figure 1B). We compared different clinicopathological features of LUAD cases stratified by the MUC3A expression level. We found that MUC3A upregulation significantly associated with an advanced pathological stage ($p < 0.05$, Figure 1C) and differentiation ($p < 0.05$, Figure 1D), all comparisons by Fisher's exact test (Table 1). Upregulation of MUC3A also associated with shorter overall survival (median survival 47.5 versus 54.5 months, 8-year follow-up, $p = 0.045$, Kaplan–Meier test; Figure 1E); however, it seemed that tumor size (diameter 4 cm, $p > 0.05$) and lymphatic metastasis status (4 lymph nodes metastasis, $p > 0.05$) were failed to present the relationship with MUC3A expression (Figure S3C-D).

Owing to mucin usually elevated expresses in adenocarcinoma, we analyzed the MUC3A and OS in patients with LUAD via the Kaplan Meier-plotter database. High expression of MUC3A was associated with poor prognosis ($p = 0.00051$, Figure 1F). To further verify the expression of MUC3A in NSCLC, 6 human NSCLC cell lines including H1975, A549, H1299, HCC827, H460 and PC9 were used to detect the expression of MUC3A by Western blotting. Lung adenocarcinoma cell lines H1975 and H1299 expressed a much higher MUC3A than any other cell lines (Figrue S3E), so we employed both cell lines for subsequent studies.

MUC3A deficiency attenuated NSCLC cell proliferation, migration, and invasion

We used lentivirus to carry MUC3A shRNAs and infected the H1975 and H1299 with 20 moi and 1 moi, respectively. WB and PCR were applied to the analysis of the knockdown effect. The stable MUC3A deficient lines were obtained (Figure 2A-B). Colony formation assay resulted indicated that MUC3A deficiency would attenuate the proliferation of H1975 and H1299 (Figure 2C). As an index reflecting cell viability, we detected Ki67 expression in MUC3A NC and MUC3A KD cells. The IF showed that the cell

viability was dramatically decreased in MUC3A deficient, CCK-8 assay also demonstrated MUC3A deficiency could impair cell growth (Figure 2D-E). Cell cycle transition was a principle factor of cell proliferation, and we analyzed the cell cycle distribution in MUC3A NC and MUC3A KD cells. The FACS results exhibited that MUC3A deficient cells were arrested at the G1/S phase with down-regulation of Cyclin D1, CDK4, and CDK6 expression (Figure 2F-G). As previously described, many mucins were able to promote cell migration and invasion. Herein, we hypothesized MUC3A could have the same function as other mucins. Transwell migration assays measured cell migration. MUC3A deficiency significantly impaired cell migration of both H1975 and H1299 cells (Figure 2H). MMP-9 was a vital metalloprotease to reflect cell invasion ability, IF the result revealed the expression of MMP-9 was notably reduced in MUC3A deficient cell (Figure 2I). WB results showed that MUC3A deficiency downregulated MMP-2 and MMP-9 expression. EMT was involved in MUC3A-mediated cell migration and invasion (Figure 2 J).

MUC3A deficiency reduced the activity of the NFκB pathway

By using the GEPIA (http://gepia.cancer-pku.cn) online tool to analyze the Pearson correlation of MUC3A and RELA log2 expression, we observed that there was no correlation between the MUC3A and RELA (Figure 3A, $p > 0.05$). Whole-cell lysis was harvested, then we detected the RELA expression in both MUC3A normal and deficient cells by WB. We found that MUC3A down-regulation did not alter the appearance of RELA (Figure 3B). Then we searched the protein-protein interaction database and found RELA could interfere with MUC3A basing on a high-throughput affinity chromatography analysis. To further verify the database results, co-immunoprecipitation was applied to investigate the interaction between RELA and MUC3A. Both cell lines expressed RELA and bound to MUC3A (Figure 3C).

As previously described, MUC3A knockdown did not affect RELA protein expression. We considered that MUC3A promoted the phosphorylation modification and nuclear translocation of RELA, and activate the NFκB pathway. Whole-cell lysis was separated into nuclear and plasma protein. WB was used to observe the phosphorylation modification and nuclear translocation of RELA, and we noted that there was a higher ration of plasma and nuclear RELA expression in MUC3A deficiency cells. However, this phenotype was not very apparent, the cells were treated with a RELA activator 10 ng/ml TNF for 30 min, and the result was more pronounced. Their rare RELA phosphorylation of the cells was detected in the absence of TNF stimulation. Upon TNF stimulation, the RELA was rapidly phosphorylated. We noticed that the RELA phosphorylation level of the MUC 3A KD group was much lower than that of the NC group, both in the nucleus and cytoplasm. (Figure 3D). We then examined the phosphorylation levels of all proteins, the phosphorylation level of MUC3A KD was lower than that of the NC group (Figure 3D). We used IF to further observed the RELA localization and phosphorylation by laser confocal microscopy. With the TNF stimulation, the RELA phosphorylation level and nuclear expression were lower in MUC3A deficient cells (Figure 3E). To further study the mechanism of NFκB pathway impairing in MUC3A deficient cells, IκB and RELA co-localization correlation coefficient were analyzed via Nikon confocal software. We investigated that the IκB and RELA laser scatter plots are more linear in MUC3A KD cells, indicating a reasonable degree of integration for IκB and RELA. This also proved to some extent that MUC3A deficiency promoted the binding of IκB to RELA, thereby inhibiting the NFκB pathway (Figure 3F). Finally,

in MUC3A deficient cells, there was less IκB binding to RELA, which suggested the NFκB pathway is attenuated by MUC3A (Figure S4A-C).

MUC3A deficiency induced more DNA damages by X-ray

Both MUC3A normal and deficient cells were irradiated with 2 Gy X-rays and then fixed for 30 min. As an index reflecting DNA double strands break, we detected γ-H2AX and 53-BP1 expression via IF. MUC3A deficiency induced more DNA structural damages and significantly promoted radiation effects (Figure 4A-B). The IF results showed that MUC3A deficiency attenuated the proliferation of H1975 and H1299 cells (Figure 4C). A higher dose of X-rays was used to overcome the sensitivity limitations of TUNEL assay; the results confirmed the synergistic effect of MUC3A deficiency and irradiation on DNA damage (Figure 4D). The survival curve was fitted in “multitarget-single hitting” model and indicated that MUC3A deficient cells posse a more radiation sensitivity character (Figure 4E-F). WB results showed that MUC3A deficient cell exposed to 2 Gy X-ray increased the expression levels of BAX and cleaved-PARP, indicating an elevation in cell death (Figure 4G).

Furthermore, DNA damage relevant proteins were also analyzed; as a result, a higher expression levels ofγ-H2AX, p-ATM, and p-ATR were presented in MUC3A deficient cells after 2 Gy irradiation, indicating that more DAN damages were detected. The BRCA1 and RAD51 repair axis was also blocked in MUC3A deficient cell. Whereas no apparent difference in XRCC5 levels was observed between MUC3A normal and deficient cells, but XRCC6 was reduced in MUC3A KD cells. We also found other pathways involved, p-P65, p-P53, and HIF-1α, were decreased to some extent in MUC3A deficient cells after 2 Gy irradiation to investigate the nuclear translocation. The whole-cell lysis was separated into nuclear and plasma protein. WB results showed that P65, P53, and GADD45 expressed less in nuclear for MUC3A deficient cells, indicating that MUC3A deficiency could inhibit nuclear translocation of P65, P53, GADD45 and attenuated the DNA damage repair. (Figure 5A-B, S5A). To verify the WB results, we investigated RAD51 and XRCC6 expression via IF, Both proteins were located in the nuclear and reduced in MUC3A KD cells (Figure S5B). MUC3A deficiency interferes with GADD45 nuclear translocation (Figure 5C). GADD45 was well known for its function of arresting the cell cycle and activated the DNA damage repair. The more binging sites of GADD45 and γ-H2AX might indicate more effect of DNA repair. We use the Nikon co-localization to analyze the binding of GADD45 and γ-H2AX, the result exhibited in the MUC3A deficient cells, less binging sites of GADD45 and γ-H2AX were observed (Figure 5D).

According to previous reports, radiation would induce autophagy and exerted a cytotoxicity effect. A novel mCherry-GFP-LC3II adenovirus was infected into the cells for 24 h and exposed to 4 Gy irradiation. As Figure S-5 C showed MUC3A deficient cells after 2 Gy irradiation-induced more red dots, indicating that more late-stage autophagy had being generated. WB result showed a higher LC3 II and lowered P62 expression in MUC3A deficient cells after irradiation (Figure S5D). More autophagic vacuole was induced in MUC3A deficient cell after irradiation (Figure S5E). However, our results unable to robustly support MUC3A facilitated radiation-sensitivity as Belin-1 and ATG-5 did not accumulate in MUC3A deficient cells.

MUC3A deficiency impaired tumor growth and promoted radiosensitivity *in vivo*

To investigate the *in vivo* effects of MUC3A deficiency, we examined the therapeutic potential of MUC3A deficiency alone or combined with radiation in the *BALB-c/Null* mice subcutaneously implanted with H1975-NC-GFP or H1975-MUC3A KD-GFP cells in the right flank. The schema was as shown in Figure 6A. Approximately two weeks after implantation, the tumor size reached 150 mm^3, and the mice received radiation or monk treatment. MUC3A deficiency significantly suppressed tumor volume, and the combination with radiation exerted synergistic effects on the reduction of the tumor burden both at Day 7 and 14 post-treatment (Figure 6B-F). Hematoxylin-eosin staining was applied to observe the morphology and pathological characters. All the masses were identified as a malignant tumor, and the shapes were similar to H1795 cells (Figure 6G).

Ki-67 staining indicated that MUC3A deficiency and radiation significantly impaired cell proliferation individually and that the combination exerted a cooperative effect *in vivo* (Figure 7A). The TUNEL assay also suggested that MUC3A deficiency and double radiation administration induced more apoptosis than the individual treatment *in vivo* (Figure 7B). Furthermore, immunohistochemistry of the tumor sections was used to verify the knockdown effect of MUC3A shRNA lentivirus infection. Xenograft model of H1975-MUC3A KD cell line presented much less MUC3A expression than that of control (Figure 7C). The same as *in vitro,* MMP-2 was notably decreased in the MUC3A deficiency cells (Figure 7D). We also noticed that HIF-1α expression was attenuated in MUC3A deficient cells after irradiation. VEGF, as the downstream of HIF-1α, was also down-regulated, suggesting that the anoxic tumor microenvironment was inhibited to some extent (Figure 7E-F).

Moreover, P65 expression did not exhibit the difference in the overview of the section. Still, in the groups with radiotherapy, MUC3A deficiency impaired the unclear translocation of P65 and presented a less total P65 expression (Figure 7G). The location and expression of P53 in xenograft model were observed as well. MUC3A normal cells expressed more P53 in the cytoplasm and nuclear, as contrast, in MUC3A deficient cells, P53 rarely expressed in the nuclear (Figure 7H). In the groups with X-ray treatment, P53 up-regulated in both MUC3A normal and deficient cells; furthermore, less unclear expression of P53 was investigated in MUC3A deficient cells.

Discussion

MUC3A is membrane-associated mucin that recent articles have reported its abnormal expression in various cancers and may involve in tumorigenesis and progression [26]. Although MUC3A had been proved and as an independent prognosticator in renal carcinoma, and our results and online database also bolster MUC3A as a pathological index to predict the clinical outcomes of LUAD. However, the molecular mechanism of MUC3A regulating tumor biological behaviors still remind unclearly. Various ways to regulate MUC3A expression. A conserved TFLK motif and hypoxia through HIF-1α would induce MUC3A expression. Epigenetically, promoter hypomethylation contributes to the expression of MUC3A in cancer cells. MUC3A shared the same SEA domain with MUC1, suggesting that its autoproteolysis must impact migration and invasion by EGF family phosphorylation. Our result also proved the lack of MUC3A dramatically impairs the migration and invasion of NSCLC cells.

In the MUC3A deficiency model, we observed that cell growth was inhibited *in vitro* and *in vivo*. Herein, we considered MUC3A knockdown might interfere cell cycle process. CyclinD1 has been reported as one downstream gene of NFκB regulating the G1/S transit via downregulating the CDK4/6, which induced cell cycle arrested and prevented S phase entry [27, 28]. FACS results presented S phase were manifestly reduced when MUC3A knockdown with decreasing expression of CyclinD1, CDK4/6. Our finding suggests that MUC3A promotes cell proliferation by aberrant regulation of G1/S checkpoint.

We searched the Integrated Interactions Database (version 2018-05) to explore the potential partner of MUC3A. RELA, also called P65, as the key number of NFκB, presented the possibility to interfere with MUC3A. Co-IP results further confirm it. NFκB is well known as a regulator to control cell growth and survival. As such, NFκB is constitutively active in various human malignant tumors [27, 29–32]. P65 nuclear translocation and phosphorylation are two crucial behaviors of the canonical activation process of the NFκB pathway [33–35]. In MUC3A deficient model, under TNF stimulation, the NFκB-p65 nuclear translocation was dramatically impaired. Meanwhile, both p-NFκB-p65 (Ser276) and p-NFκB-p65 (Ser536) were dephosphorylated in the cytoplasm and nuclear. Furthermore, we investigated more IκB protein bound to P65. Based on the above results, we put forward a particular model of MUC3A interaction with NF-kB in NSCLC. MUC3A may be crucial for constitutive phosphorylation of P65. Therefore, compared to negative control, p-NFκB-p65 (Ser276) was dephosphorylated in MUC3A deficient cells, and P65 bound to IκBβ again to increase their stability. The mechanism of the phosphorylation of P65 via MUC3A still reminded unclearly. We hypothesized IκBβ might inhibit the phosphorylation of NFκBp65 (Ser276) as the binding site of IκBβ is close to Thr276 in P65. Moreover, the phosphorylation of NFκB-p65 (Ser536) was nobly attenuated in MUC3A deficient NSCLC cells. The findings indicate that the interaction of MUC3A and p65 is essential to induce phosphorylation of P65, thereby promoting nuclear translocation of P65 and mediating NFκB activation in NSCLC cells.

High energy X-rays inflicts cellular damages directly via ionizing water molecules and producing hydroxyl radicals, and indirectly via attacking the DNA [36]. IR can induce various forms of DNA damage, compared with other types of DNA damages caused by IR, DSBs are determinant of cellular radiosensitivity. 53BP1, GADD45, and γH2AX are the indexes that exhibit DNA linkage and reflect DNA damage [37–40]. Homologous recombination repair (HRR) and non-homologous end-joining (NHEJ) are two major methods to repair DSBs. In mammalian cells, HRR performs most DSBs, BRCA/Rad axis is active by p-ATM and plays a vital role in repairing DNA damage [41, 42], our findings showed an obvious interruption of BRCA/Rad axis. XRCCs are involved in NHEJ, and MUC3A deficiency also regulate XRCCs as NHEJ most conduct DSBs repair [43], however, in H1975 cells, XRCCs weren't downregulated which suggest that XRCCs may be a passage gene in MUC3A induced DNA damage repair impairing. It is reported that NFκB signaling has anti-apoptotic effects and involved in DNA damage repair, MUC3Ainduced NFκB activation plays a potent role in radiation resistance for NSCLC cells, and our result presented NFκB activation was inhibited in MUC3A deficiency model after irradiation. In this study, MUC3A knockdown remarkably down-regulated BRCA1, RAD51, and P53 nuclear translocation, suggesting radiosensitive was promoted by suppression of DNA damage repair and activation of pro-apoptotic proteins. Thus, this revealed a potential mechanism for radiosensitive enhancement.

Furthermore, we have revealed that MUC3A would induce angiogenesis in NSCLC via elevating the expression of VEGF. In this study, we assume VEGF was regulated in two ways. It has been reported that NFκB signaling induces angiogenesis by increasing the production of VEGF [44–46], angiogenesis induced by MUC3A is also mediated by NFκB activation in NSCLC. Radiation-mediate hypoxia triggers HIF-1α transcription and up-regulates VEGF expression [46, 47], MUC3A knockdown may enhance radiosensitivity by promoting oxygen stress and impair HIF-1α and VEGF expression level. Furthermore, MMP-2 and MMP-9 are also known to stimulate tumor angiogenesis and the epithelial-to-mesenchymal transition (EMT) through partial proteolysis of the ECM [48–52]. Our results failed to detect NSCLC cell EMT; however, cell-cell attachment showed closer in MUC3A deficient cells. The alterations suggest that MUC3A promotes the migration and invasion of NSCLC cells in various ways. Previous studies indicated that tumor invasiveness is remarkably increased in patients with high mucin expression. We found high MUC3A expression was a trend to indicate more lymph nodes metastasis; however, as the limitation of samples, our finding failed to show the association between MUC3A and tumor metastasis in tissue microarray.

Finally, our studies indicated that MUC3A promoted tumorigenesis via activating the NFκB pathway and impaired X-ray response via interrupting DNA damage repair. Its high expression was associated with unfavorable clinical outcomes in patients with lung adenocarcinoma, who should be more frequent follow-up and might benefit less from radiotherapy.

Conclusion

MUC3A as a potential oncogene, is associated with unfavorable clinical outcomes via targeting NFκB pathway. Of note, MUC3A participates the radiation-resistance in lung adenocarcinoma. Patient with high expression levels of MUC3A should be more frequent follow-up and might benefit less from radiotherapy.

Abbreviations

NSCLC
Non-Small Cell Lung Cancer; LUAD:Lung Adenocarcinoma; BED:Biological Effect Dosage; MUC3A:Mucin 3A; DFS:Disease Free Survival; OS:Overall Survival; RELA/P65:Reticuloendotheliosis Viral Oncogene Homolog A; TUNEL:TdT-Mediated dUTP Nick-End Labeling; WB:Western Blotting; IHC:Immunohistochemistry; PCR:Polymerase Chain Reaction; GAPDH:Glyceraldehyde-3-Phosphate Dehydrogenase; CDK4/6:Cyclin-Dependent Kinase 4/6; P21:Cyclin Dependent Kinase Inhibitor 1A; ICAM1:Intercellular Adhesion Molecule 1; MMP:Matrix Metallopeptidase; EMT:Epithelial-Mesenchymal Transition; IκB:Inhibitor of Nuclear Factor Kappa B Kinase Subunit; TNF:Tumor Necrosis Factor; PARP:Poly (ADP-ribose) polymerase; DSB:Double Strand Break; 53BP1:P53 Binding Protein 1; γ-H2AX:γ-H2A Histone Family Member X; BRCA1:Breast Cancer Susceptibility Genes 1; RAD51:RAD51 Recombinase; XRCC:X-ray Repair Cross Complementing; ATM:Ataxia Telangiectasia Mutated; ATR:Ataxia Telangiectasia and Rad 3 Related; HIF1α:Hypoxia Inducible Factor-1; GADD45:Growth Arrest and DNA Damage Inducible Protein 45; BCL2:B Cell Lymphoma-2; BAX:BCL-2 Associated X Protein;

P62:Sequestosome-1; LC3:Microtubule-Associated Protein 1 Light Chain 3; ATG5:Autophagy Related 5; VEGF:Vascular Endothelial Growth Factor

Declarations

Ethics approval and consent to participate

This study was approved by the Medical Ethics Committee at Zhongnan Hospital of Wuhan University and the Institutional Animal Care and Use Committee of Wuhan University.

Consent for publication

All co-authors reviewed the manuscript and agreed to publish.

Availability of data and materials

The authors confirm that the data supporting the findings of this study are available within the article and its supplementary materials.

Competing Interests

The authors have declared that no competing interest exists.

Funding

This study was supported by National Natural Science Foundation of China (81773236, 81800429 and 81972852), Health Commission of Hubei Province Medical Leading Talent Project and Scientific Research Project (WJ2019H002 and WJ2019Q047), Young & Middle-Aged Medical Backbone Talents of Wuhan City (WHQG201902), Zhongnan Hospital of Wuhan University Science, Technology and Innovation Seed Fund (znpy2018028, znpy2018070, znpy2019001, znpy2019028 and ZNJC201922), the Sailing Fund of Fujian Medical University (No.2018QH1164), and the Scientific Fund of Sanming Science and Technology Bureau (N0.2018-5-1(7)).

Authors' contributions

YS, YG and CX conceived and designed the experiments. YS, XS, CY, SM, YL, SP and FT performed the experiments in vitro. YS, XS, CY, XT, FW, ZH and HY performed the experiments in vivo. YS, YX, XW, JZ, YG and CX analyzed the results. YS, XS and CY contributed to the writing of the manuscript. YS, YG and CX polished the language.

Acknowledgements

Special thanks to all the staffs and faculties in the Department of Medical and Radiation, Zhongnan Hospital of Wuhan University for their generous help for irradiating the cells and animals.

References

1. Torre LA, Bray F, Siegel RL, Ferlay J, Lortet-Tieulent J, Jemal A. Global cancer statistics, 2012. CA Cancer J Clin. 2015; 65: 87-108.
2. Siegel RL, Miller KD, Jemal A. Cancer statistics, 2016. CA Cancer J Clin. 2016; 66: 7-30.
3. Politi K, Herbst RS. Lung cancer in the era of precision medicine. Clin Cancer Res. 2015; 21: 2213-20.
4. Chen W, Zheng R, Baade PD, Zhang S, Zeng H, Bray F, et al. Cancer statistics in China, 2015. CA Cancer J Clin. 2016; 66: 115-32.
5. Lazzari C, Bulotta A, Ducceschi M, Vigano MG, Brioschi E, Corti F, et al. Historical Evolution of Second-Line Therapy in Non-Small Cell Lung Cancer. Front Med (Lausanne). 2017; 4: 4.
6. Auperin A, Le Pechoux C, Rolland E, Curran WJ, Furuse K, Fournel P, et al. Meta-analysis of concomitant versus sequential radiochemotherapy in locally advanced non-small-cell lung cancer. J Clin Oncol. 2010; 28: 2181-90.
7. Machtay M, Paulus R, Moughan J, Komaki R, Bradley JE, Choy H, et al. Defining local-regional control and its importance in locally advanced non-small cell lung carcinoma. J Thorac Oncol. 2012; 7: 716-22.
8. De Ruysscher D, Faivre-Finn C, Nestle U, Hurkmans CW, Le Pechoux C, Price A, et al. European Organisation for Research and Treatment of Cancer recommendations for planning and delivery of high-dose, high-precision radiotherapy for lung cancer. J Clin Oncol. 2010; 28: 5301-10.
9. Le Chevalier T, Arriagada R, Quoix E, Ruffie P, Martin M, Tarayre M, et al. Radiotherapy alone versus combined chemotherapy and radiotherapy in nonresectable non-small-cell lung cancer: first analysis of a randomized trial in 353 patients. J Natl Cancer Inst. 1991; 83: 417-23.
10. Martel MK, Ten Haken RK, Hazuka MB, Kessler ML, Strawderman M, Turrisi AT, et al. Estimation of tumor control probability model parameters from 3-D dose distributions of non-small cell lung cancer patients. Lung Cancer. 1999; 24: 31-7.
11. Van Klinken BJ, Einerhand AW, Buller HA, Dekker J. Strategic biochemical analysis of mucins. Anal Biochem. 1998; 265: 103-16.
12. Kufe DW. Mucins in cancer: function, prognosis and therapy. Nat Rev Cancer. 2009; 9: 874-85.
13. Awaya H, Takeshima Y, Yamasaki M, Inai K. Expression of MUC1, MUC2, MUC5AC, and MUC6 in atypical adenomatous hyperplasia, bronchioloalveolar carcinoma, adenocarcinoma with mixed subtypes, and mucinous bronchioloalveolar carcinoma of the lung. Am J Clin Pathol. 2004; 121: 644-53.
14. Situ D, Wang J, Ma Y, Zhu Z, Hu Y, Long H, et al. Expression and prognostic relevance of MUC1 in stage IB non-small cell lung cancer. Med Oncol. 2011; 28 Suppl 1: S596-604.
15. Wu G, Kim D, Kim JN, Park S, Maharjan S, Koh H, et al. A Mucin1 C-terminal Subunit-directed Monoclonal Antibody Targets Overexpressed Mucin1 in Breast Cancer. Theranostics. 2018; 8: 78-91.
16. Tsutsumida H, Goto M, Kitajima S, Kubota I, Hirotsu Y, Wakimoto J, et al. MUC4 expression correlates with poor prognosis in small-sized lung adenocarcinoma. Lung Cancer. 2007; 55: 195-203.

17. Yu CJ, Shih JY, Lee YC, Shun CT, Yuan A, Yang PC. Sialyl Lewis antigens: association with MUC5AC protein and correlation with post-operative recurrence of non-small cell lung cancer. Lung Cancer. 2005; 47: 59-67.
18. Gum JR, Jr., Ho JJ, Pratt WS, Hicks JW, Hill AS, Vinall LE, et al. MUC3 human intestinal mucin. Analysis of gene structure, the carboxyl terminus, and a novel upstream repetitive region. J Biol Chem. 1997; 272: 26678-86.
19. Copin MC, Devisme L, Buisine MP, Marquette CH, Wurtz A, Aubert JP, et al. From normal respiratory mucosa to epidermoid carcinoma: expression of human mucin genes. Int J Cancer. 2000; 86: 162-8.
20. Duncan TJ, Watson NF, Al-Attar AH, Scholefield JH, Durrant LG. The role of MUC1 and MUC3 in the biology and prognosis of colorectal cancer. World J Surg Oncol. 2007; 5: 31.
21. Park HU, Kim JW, Kim GE, Bae HI, Crawley SC, Yang SC, et al. Aberrant expression of MUC3 and MUC4 membrane-associated mucins and sialyl Le(x) antigen in pancreatic intraepithelial neoplasia. Pancreas. 2003; 26: e48-54.
22. Rakha EA, Boyce RW, Abd El-Rehim D, Kurien T, Green AR, Paish EC, et al. expression of mucins (MUC1, MUC2, MUC3, MUC4, MUC5AC and MUC6) and their prognostic significance in human breast cancer. Mod Pathol. 2005; 18: 1295-304.
23. Wang RQ, Fang DC. Alterations of MUC1 and MUC3 expression in gastric carcinoma: relevance to patient clinicopathological features. J Clin Pathol. 2003; 56: 378-84.
24. Shibahara H, Higashi M, Yokoyama S, Rousseau K, Kitazono I, Osako M, et al. A comprehensive expression analysis of mucins in appendiceal carcinoma in a multicenter study: MUC3 is a novel prognostic factor. PLoS One. 2014; 9: e115613.
25. Arul GS, Moorghen M, Myerscough N, Alderson DA, Spicer RD, Corfield AP. Mucin gene expression in Barrett's oesophagus: an in situ hybridisation and immunohistochemical study. Gut. 2000; 47: 753-61.
26. Yonezawa S, Higashi M, Yamada N, Yokoyama S, Kitamoto S, Kitajima S, et al. Mucins in human neoplasms: clinical pathology, gene expression and diagnostic application. Pathol Int. 2011; 61: 697-716.
27. Zhong H, Voll RE, Ghosh S. Phosphorylation of NF-kappa B p65 by PKA stimulates transcriptional activity by promoting a novel bivalent interaction with the coactivator CBP/p300. Mol Cell. 1998; 1: 661-71.
28. Zheng K, He Z, Kitazato K, Wang Y. Selective Autophagy Regulates Cell Cycle in Cancer Therapy. Theranostics. 2019; 9: 104-25.
29. Vermeulen L, De Wilde G, Van Damme P, Vanden Berghe W, Haegeman G. Transcriptional activation of the NF-kappaB p65 subunit by mitogen- and stress-activated protein kinase-1 (MSK1). EMBO J. 2003; 22: 1313-24.
30. Geng H, Wittwer T, Dittrich-Breiholz O, Kracht M, Schmitz ML. Phosphorylation of NF-kappaB p65 at Ser468 controls its COMMD1-dependent ubiquitination and target gene-specific proteasomal elimination. EMBO Rep. 2009; 10: 381-6.

31. Jang HD, Yoon K, Shin YJ, Kim J, Lee SY. PIAS3 suppresses NF-kappaB-mediated transcription by interacting with the p65/RelA subunit. J Biol Chem. 2004; 279: 24873-80.
32. Zhu Y, Zhang M, Luo L, Gill MR, De Pace C, Battaglia G, et al. NF-kappaB hijacking theranostic Pt(II) complex in cancer therapy. Theranostics. 2019; 9: 2158-66.
33. Hochrainer K, Racchumi G, Zhang S, Iadecola C, Anrather J. Monoubiquitination of nuclear RelA negatively regulates NF-kappaB activity independent of proteasomal degradation. Cell Mol Life Sci. 2012; 69: 2057-73.
34. Higashitsuji H, Higashitsuji H, Nagao T, Nonoguchi K, Fujii S, Itoh K, et al. A novel protein overexpressed in hepatoma accelerates export of NF-kappa B from the nucleus and inhibits p53-dependent apoptosis. Cancer Cell. 2002; 2: 335-46.
35. Strebovsky J, Walker P, Lang R, Dalpke AH. Suppressor of cytokine signaling 1 (SOCS1) limits NFkappaB signaling by decreasing p65 stability within the cell nucleus. FASEB J. 2011; 25: 863-74.
36. Irminger-Finger I, Ratajska M, Pilyugin M. New concepts on BARD1: Regulator of BRCA pathways and beyond. Int J Biochem Cell Biol. 2016; 72: 1-17.
37. Prakash R, Zhang Y, Feng W, Jasin M. Homologous recombination and human health: the roles of BRCA1, BRCA2, and associated proteins. Cold Spring Harb Perspect Biol. 2015; 7: a016600.
38. Kujjo LL, Laine T, Pereira RJ, Kagawa W, Kurumizaka H, Yokoyama S, et al. Enhancing survival of mouse oocytes following chemotherapy or aging by targeting Bax and Rad51. PLoS One. 2010; 5: e9204.
39. Gasparini P, Lovat F, Fassan M, Casadei L, Cascione L, Jacob NK, et al. Protective role of miR-155 in breast cancer through RAD51 targeting impairs homologous recombination after irradiation. Proc Natl Acad Sci U S A. 2014; 111: 4536-41.
40. Barbano R, Copetti M, Perrone G, Pazienza V, Muscarella LA, Balsamo T, et al. High RAD51 mRNA expression characterize estrogen receptor-positive/progesteron receptor-negative breast cancer and is associated with patient's outcome. Int J Cancer. 2011; 129: 536-45.
41. Pace P, Mosedale G, Hodskinson MR, Rosado IV, Sivasubramaniam M, Patel KJ. Ku70 corrupts DNA repair in the absence of the Fanconi anemia pathway. Science. 2010; 329: 219-23.
42. Li H, Vogel H, Holcomb VB, Gu Y, Hasty P. Deletion of Ku70, Ku80, or both causes early aging without substantially increased cancer. Mol Cell Biol. 2007; 27: 8205-14.
43. Goudelock DM, Jiang K, Pereira E, Russell B, Sanchez Y. Regulatory interactions between the checkpoint kinase Chk1 and the proteins of the DNA-dependent protein kinase complex. J Biol Chem. 2003; 278: 29940-7.
44. Lee JC, Tae HJ, Kim IH, Cho JH, Lee TK, Park JH, et al. Roles of HIF-1alpha, VEGF, and NF-kappaB in Ischemic Preconditioning-Mediated Neuroprotection of Hippocampal CA1 Pyramidal Neurons Against a Subsequent Transient Cerebral Ischemia. Mol Neurobiol. 2017; 54: 6984-98.
45. Mo SJ, Hong J, Chen X, Han F, Ni Y, Zheng Y, et al. VEGF-mediated NF-kappaB activation protects PC12 cells from damage induced by hypoxia. Neurosci Lett. 2016; 610: 54-9.

46. Li Y, Sui H, Jiang C, Li S, Han Y, Huang P, et al. Dihydroartemisinin Increases the Sensitivity of Photodynamic Therapy Via NF-kappaB/HIF-1alpha/VEGF Pathway in Esophageal Cancer Cell in vitro and in vivo. Cell Physiol Biochem. 2018; 48: 2035-45.
47. Zhang X, Qi Z, Yin H, Yang G. Interaction between p53 and Ras signaling controls cisplatin resistance via HDAC4- and HIF-1alpha-mediated regulation of apoptosis and autophagy. Theranostics. 2019; 9: 1096-114.
48. Vandooren J, Van den Steen PE, Opdenakker G. Biochemistry and molecular biology of gelatinase B or matrix metalloproteinase-9 (MMP-9): the next decade. Crit Rev Biochem Mol Biol. 2013; 48: 222-72.
49. Kobayashi T, Kim H, Liu X, Sugiura H, Kohyama T, Fang Q, et al. Matrix metalloproteinase-9 activates TGF-beta and stimulates fibroblast contraction of collagen gels. Am J Physiol Lung Cell Mol Physiol. 2014; 306: L1006-15.
50. Tranchant I, Vera L, Czarny B, Amoura M, Cassar E, Beau F, et al. Halogen bonding controls selectivity of FRET substrate probes for MMP-9. Chem Biol. 2014; 21: 408-13.
51. Apoorv TS, Babu PP, Meese S, Gai PP, Bedu-Addo G, Mockenhaupt FP. Matrix metalloproteinase-9 polymorphism 1562 C > T (rs3918242) associated with protection against placental malaria. Am J Trop Med Hyg. 2015; 93: 186-8.
52. Li M, Yang G, Xie B, Babu K, Huang C. Changes in matrix metalloproteinase-9 levels during progression of atrial fibrillation. J Int Med Res. 2014; 42: 224-30.

Tables

Table 1 The corelation between MUC3A expression and clinicopathological characteristics

	MUC3a		N	p-value
	low	high		
Gender				
Male	38	13	51	0.300
Female	35	6	41	
	73	19		
Age				
≦60	37	1	38	0.000
>60	36	18	54	
Tumor size (cm)				
<4	33	12	45	0.623
≥4	23	11	34	
None	7	6		
Histological grade				
I/I-II	5	2	7	0.039
II	43	7	50	
II-III/III	22	9	31	
I-III	3	1	4	
Clinical Stage				
I	20	3	23	0.045
II	15	3	18	
III-IV	18	8	26	
Non	18	7	25	
Lymph node status				
4	23	2	25	0.149

≥4	48	12	60	
Non	2	5	7	
Carcinoma				
Primary	73	19	92	
Adjacent	89	0	89	
ALK	67	17	84	0.111
positive	61	13	74	
negative	6	4	10	
Non	6	2	8	
EGFR	73	19	92	0.553
positive	17	4	21	
negative	56	15	71	

Figures

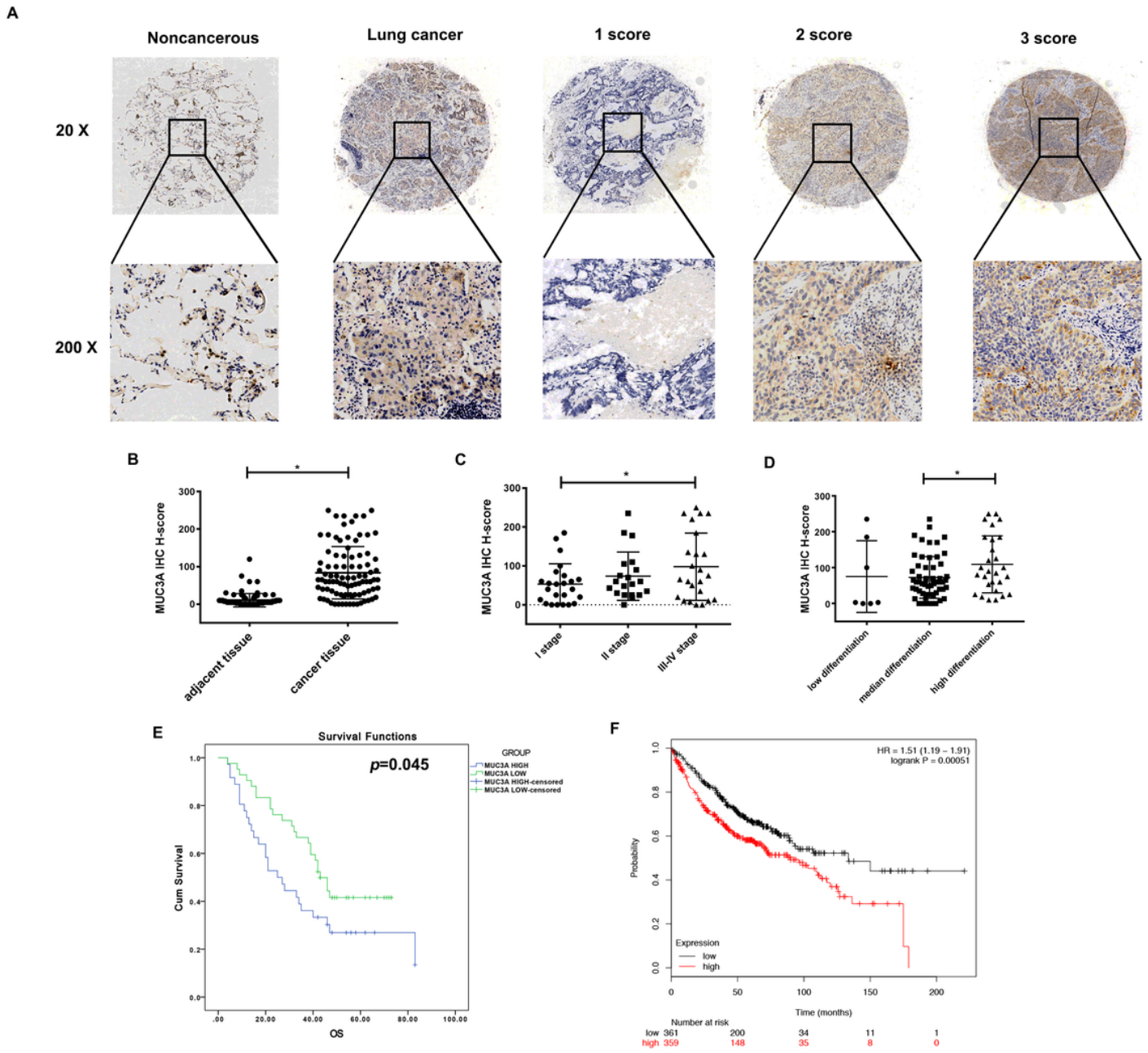

Figure 1

MUC3A was highly expressed in lung cancer and relevant to the poor OS in database and tissue microarray. (A) The 20× and 200× representative images of IHC. (B) The expression levels of MUC3A protein were significantly higher in NSCLC tissues than those in the paired normal tissues. The tissue microarray results included 92 pairs ($p < 0.001$, paired t-test). (C) MUC3A expression levels in lung cancer tissues subgrouped by staging ($p < 0.001$, ANOVA). (D) MUC3A expression levels in lung cancer tissues subgrouped by differentiation ($p < 0.001$, ANOVA). (E) Kaplan–Meier plot of 92 patients with survival data (from tissue arrays) stratified by MUC3A expression levels. Patients expressing less MUC3A displayed higher overall survival than the other patients ($p = 0.045$, Kaplan–Meier survival test). (F) Kaplan–Meier

plot of 720 patients with survival data (from www.kmplot.com) stratified by MUC3A mRNA levels. Patients expressing more MUC3A displayed shorter overall survival than the other patients (p = 0.00051, Kaplan–Meier survival test).

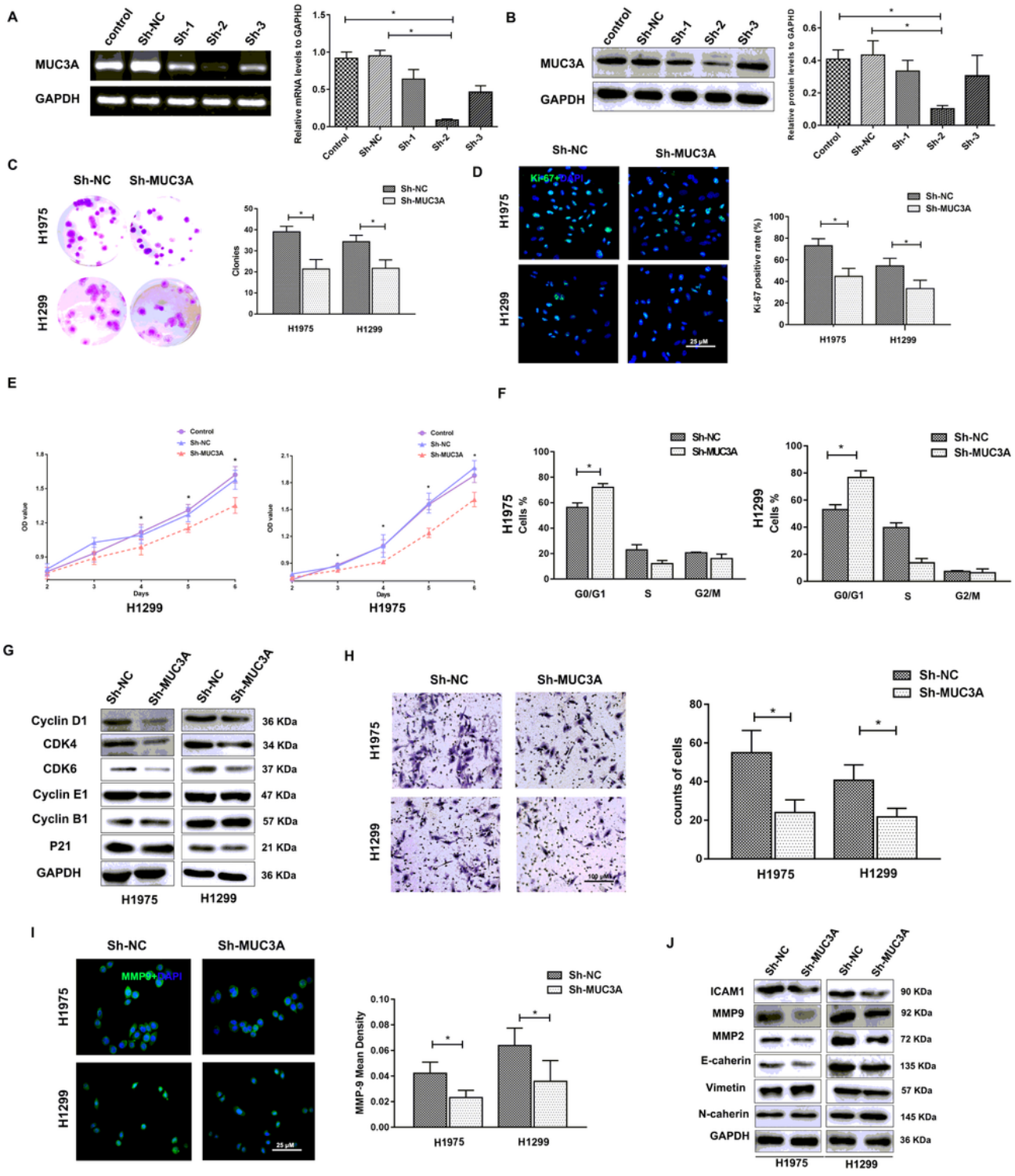

Figure 2

MUC3A deficiency attenuated NSCLC cell proliferation, migration, and invasion. (A) PCR analysis to detect the knockdown effects of different shRNAs. shRNA-2 was more efficient than the others. The

mRNA levels were standardized with GAPDH. All values shown were mean ± SD of triplicate measurements and repeated 3 times. *, $p < 0.05$. (B) WB analysis to detect the knockdown effects of different shRNAs. ShRAN-2 was more efficient than the others. The protein levels were standardized with GAPDH. (C) Representative images of crystal violet stain on Day 15. *, $p < 0.05$. (D) Representative images of Ki-67 IF staining in H1975 and H1299 cells. The MUC3A deficiency group had less Ki-67 positive foci (green) than the control group. Scale bar, 25 μm. *, $p < 0.05$. (E) CCK array to detect cell proliferation. *, $p < 0.05$. (F) FACS analysis to detect the cell cycle distribution. More cells in the MUC3A deficiency group were arrested at G0/G1. *, $p < 0.05$. (G) Western blotting analysis of protein abundance involved in cell cycle checkpoints, including Cyclin D1, CDK4, CDK6, Cyclin E1, Cyclin B1, p21. (H) Transwell assay for cell migration and invasion. The MUC3A deficiency group had significantly less migration and invasion cells than the control group. *, $p < 0.05$. (I) Representative images of MMP9 IF staining in H1975 and H1299 cells. MUC3A knockdown reduced MMP9 expression. *, $p < 0.05$. (J) Western blotting analysis of protein abundance involved in cell migration and EMT, including ICAM1, MMP2, MMP9, E-cadherin, Vimentin, and N-cadherin.

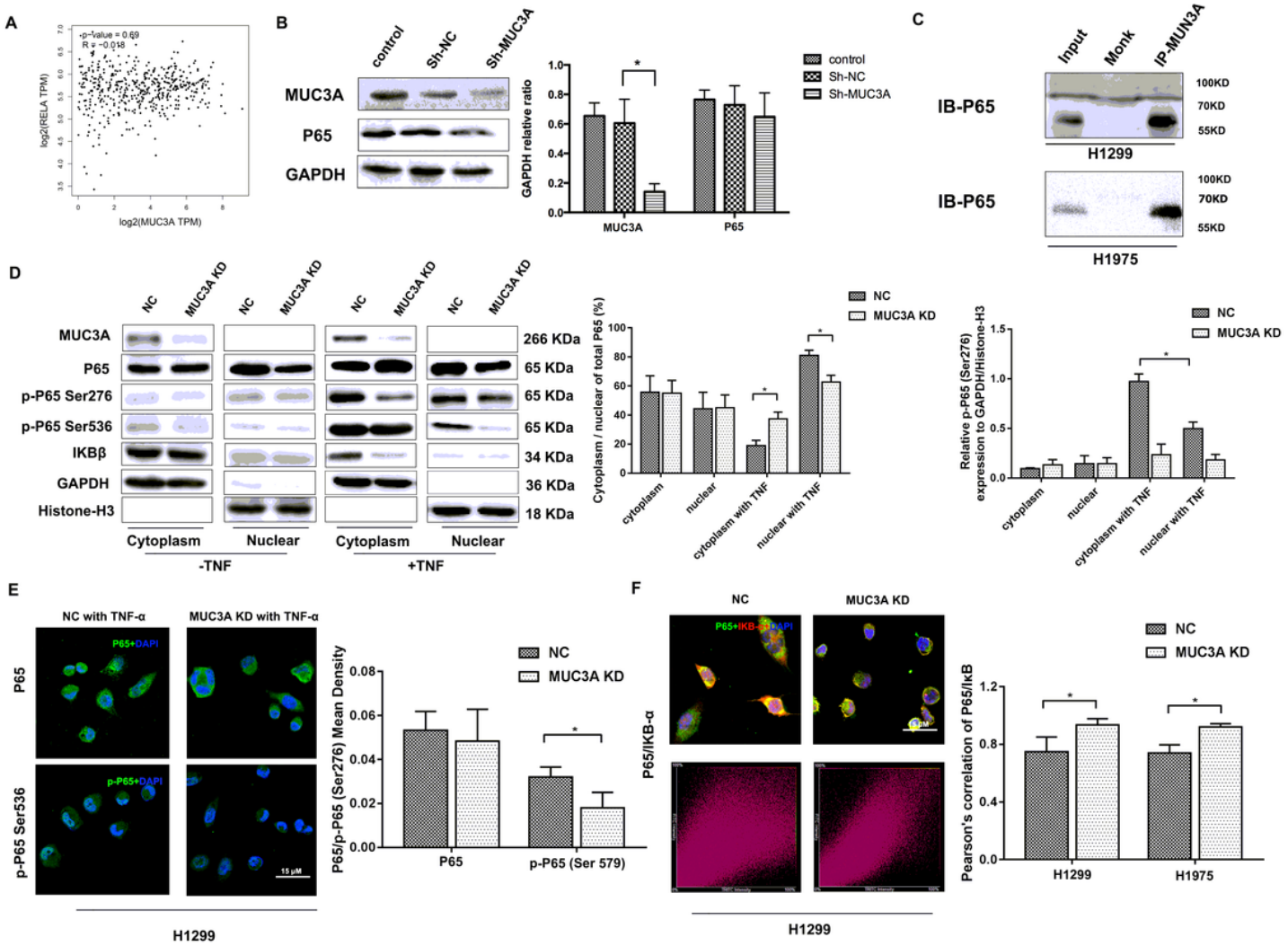

Figure 3

MUC3A deficiency reduced the activity of the NF-κB pathway. (A) R language package to analyze Pearson correlation of MUC3A and RELA log2 expression, database from http://gepia.cancer-pku.cn. p = 0.69, R = -0.018. (B) WB to detect the relationship between MUC3A and p65. p65 whole protein expression did not interfere with MUC3A, p > 0.05. (C) Co-IP to analyze the binding of MUC3A and p65. The representative images exhibited that MUC3A was linked to p65. (D) WB was used to investigate the MUC3A, p65, p-p65, IκB, GAPDH, and Histone H3. There was more plasm p65 expression in MUC3A knockdown cells after 30 mins TNF disposal. *, p < 0.05. In both plasm and nuclear, MUC3A deficiency attenuated the phosphorylation levels of p65. *, p < 0.05. (E) Representative images of p65 and p-p65 IF staining in H1299 cells. The MUC3A deficiency group had less p-p65 positive staining (green) than the control group. *, p < 0.05. For total p65, the statistical difference was not significant between the control and MUC3A deficiency groups. *, p < 0.05. (F) IF to detect the binding condition of p65 (green) and IκB (red). Nikon laser confocal software NIS-element ts ar 3.1 was used to analysis the colocalization. The scatter image presented the correlation of fluorescence intensity between FITC and TRITC. MUC3A deficiency increased colocalization of p65 and IκB.

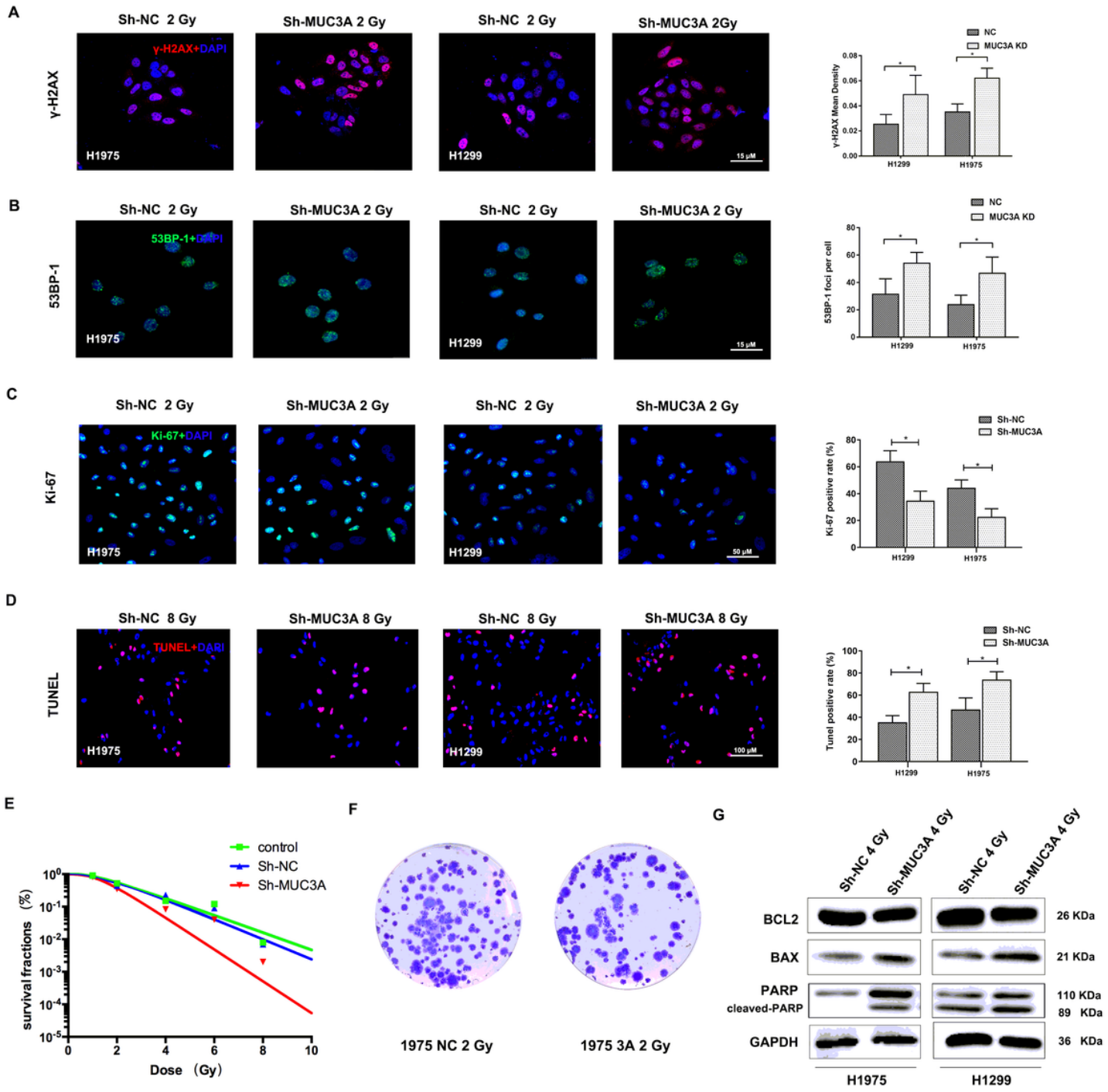

Figure 4

MUC3A deficiency induced more DNA damages by X-ray. (A) Representative images of γ-H2AX IF staining in H1975 and H1299 cells. The MUC3A deficiency cells with 2 Gy radiation had more γ-H2AX (red) positive foci than the control. All values shown were mean ± SD of triplicate measurements and repeated 3 times. *, $p < 0.05$. (B) Representative images of 53BP1 IF staining in H1975 and H1299 cells. The MUC3A deficiency cells with 2 Gy radiation had more 53BP1 (green) positive foci than control. *, $p < 0.05$. (C) Representative images of Ki67 IF staining in H1975 and H1299 cells. The MUC3A deficiency cells with

2 Gy radiation had less Ki67 positive foci (green) than the control. *, p < 0.05. (D) Representative images of TUNEL staining in H1975 and H1299 cells. The MUC3A deficiency cells with 8 Gy radiation had more TUNEL staining (red) than individual treatment. *, p < 0.05. (D) The multitarget-single hitting model was used to fit the survival curve. The survival fraction of MUC3A deficiency cells was significantly lower than that of the control groups. (F) Representative crystal violet staining photos of H1975 parental and MUC3A knockdown cells with 2 Gy irradiation. (G) Western blotting analysis of BLC2, BAX, and PARP protein levels in H1975 and H1299 parental and MUC3A knockdown cells.

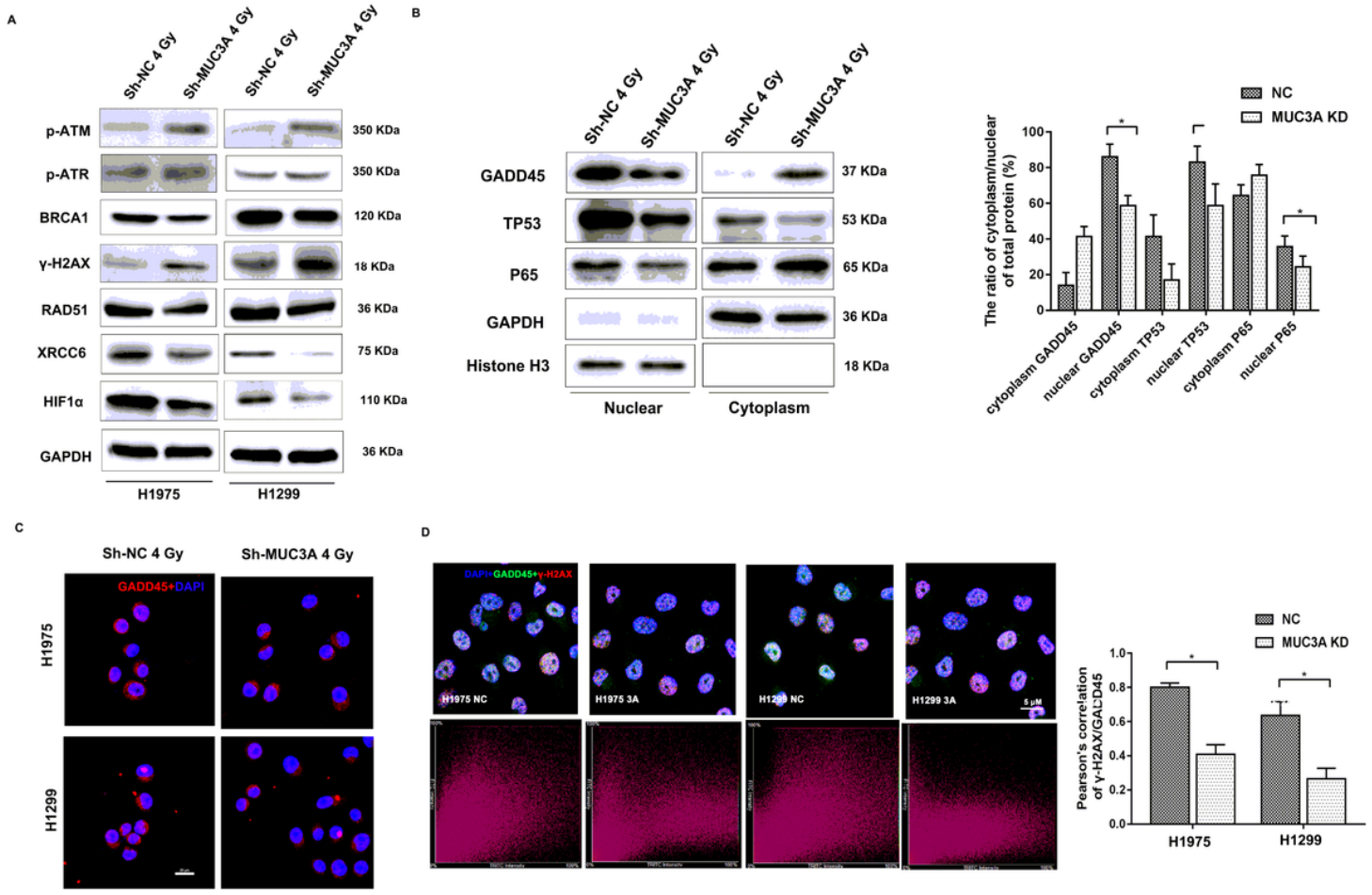

Figure 5

The mechanism of MUC3A deficiency induced more DNA damages by X-ray. (A) Western blotting analysis of p-ATM, p-ATR, γ-H2AX, BRCA1, RAD51, XCRR6, and HIF1α protein levels in H1975 and H1299 parental and MUC3A knockdown cells after 4 Gy irradiation. (B) WB analysis to investigate the plasm and nuclear protein levels of GADD45, TP53, and p65. There were less nuclear GADD45, TP53, and p65 in MUC3A knockdown cells after 4 Gy irradiation. *, p < 0.05. (C) Representative images of GADD45 in H1975 and H1299 cells after 4 Gy irradiation. The MUC3A deficiency group had less GADD45 foci (red) in the nuclear (blue) than the control group. *, p < 0.05. (D) As previously described, specific software was used to

analyze the colocalization of γ-H2AX and DADD45. In MUC3A deficiency cells, less DADD45 was recruited to γ-H2AX. *, p < 0.05.

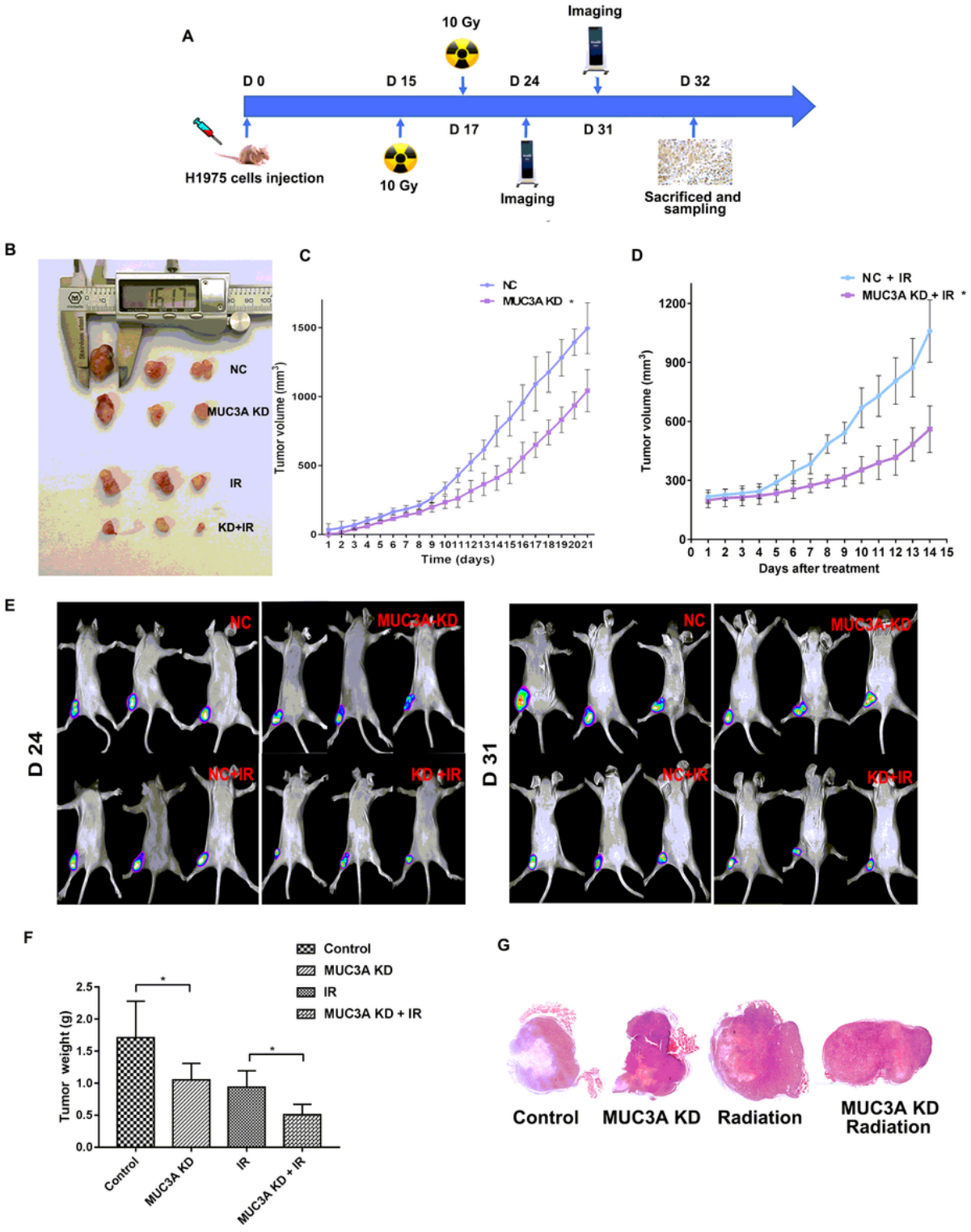

Figure 6

MUC3A deficiency impaired tumor growth and promoted radiosensitivity in vivo. (A) Treatment schema. (B) Gross view of the tumors. (C) Growth curve of tumor volume for the group without radiotherapy. *, p < 0.05, MUC3A deficiency vs. control. (D) Growth curve of tumor volume for the group with radiotherapy. *,

p < 0.05, MUC3A deficiency vs. control. (E) In vivo imaging of the size and destiny of GFP-H1975 cells at Day 24 and 31. (F) Tumor weight was significantly different between the control and MUC3A deficiency groups with or without radiotherapy. *, p < 0.05. (G) Hematoxylin-eosin staining was applied to investigate the morphology and pathological characters. All the masses were identified as a malignant tumor, and the shapes were similar to H1795 cells. More necrosis was observed in the control group.

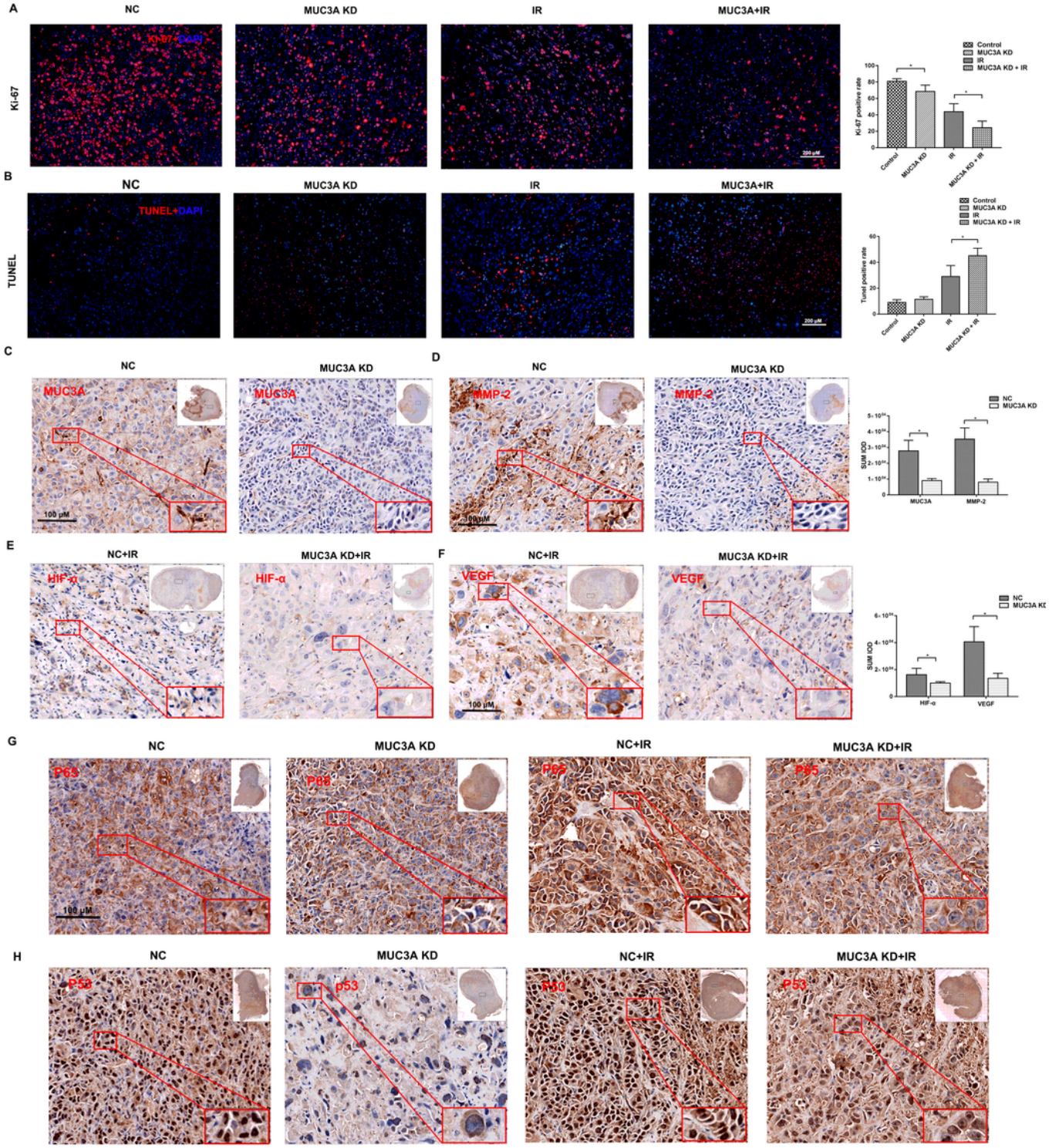

Figure 7

MUC3A presented a comprehensive anti-tumor effect in vivo. (A) Representative images of Ki-67 IF staining in tumor tissues. The MUC3A deficient cells had less Ki67 positive cells (red) than the MUC3A normal cells with or without radiotherapy. *, $p < 0.05$. (B) Representative images of TUNEL staining in tumor tissues. The MUC3A deficient cells had more DNA linkage (red) than the MUC3A normal cells with or without radiotherapy. *, $p < 0.05$. (C) Representative IHC images of MUC3A. The MUC3A deficient cells had less MUC3A expression than the control. *, $p < 0.05$. (D) Representative IHC images of MMP2. The MUC3A deficient cells had less MMP2 expression than the control. *, $p < 0.05$. (E) Representative IHC images of HIF1α. The MUC3A deficient cells had less HIF-1α expression than the control. *, $p < 0.05$. (F) Representative IHC images of VEGF. The MUC3A deficient cells had less VEGF expression than the control. *, $p < 0.05$. (G) Representative IHC images of P65. The MUC3A deficient cells had less p65 expression in nuclear with or without radiotherapy. (H) Representative IHC images of TP53. The MUC3A deficient cells had less TP53 expression in nuclear with or without radiotherapy.

Supplementary Files

This is a list of supplementary files associated with this preprint. Click to download.

- Manuscriptyg20200810.pdf
- Manuscriptyg20200810.pdf
- SupplementaryMaterialyg20200810.docx
- SupplementaryMaterialyg20200810.docx